RSC Advances

PAPER

View Article Online
View Journal | View Issue

Cite this: *RSC Adv.*, 2022, **12**, 35436

Cellulose nanocrystals isolated from corn leaf: straightforward immobilization of silver nanoparticles as a reduction catalyst†

Roya Thach-Nguyen,[ab] Hoa-Hung Lam,[ab] Hong-Phuong Phan[ab] and Trung Dang-Bao *[ab]

As the most abundant natural biopolymer on earth, celluloses have long-term emerged as a capable platform for diverse purposes. In the context of metal nanoparticles applied to catalysis, the alternatives to traditional catalyst supports by using biomass-derived renewable materials, likely nanocelluloses, have been paid a great effort, in spite of being less exploited. In this study, cellulose nanocrystals were isolated from corn leaf *via* chemical treatment involving alkalizing, bleaching and acid hydrolysis. The crystallinity of obtained cellulose was evaluated in each step, focusing on the effects of reactant concentration and reaction time. Cellulose nanocrystals were characterized by powder X-ray diffraction (XRD), Fourier-transform infrared spectroscopy (FT-IR), transmission electron microscopy (TEM), evidencing the presence of cellulose nanospheres (crystallinity index of 67.3% in comparison with 38.4% from untreated raw material) in the size range of 50 nm. Without using any additional surfactants or stabilizers, silver nanoparticles (AgNPs) well-dispersed on the surface of cellulose nanocrystals (silver content of 5.1 wt%) could be obtained by a simple chemical reduction using $NaBH_4$ at room temperature. The catalytic activity was evaluated in the selective reductions of 4-nitrophenol towards 4-aminophenol and methyl orange towards aromatic amine derivatives in water at room temperature. The effects of catalyst amount and reaction time were also studied in both reduction processes, showing near-quantitative conversions within 5 minutes and obeying the pseudo-first-order kinetics, with the apparent kinetic rate constants of 8.9×10^{-3} s^{-1} (4-nitrophenol) and 13.6×10^{-3} s^{-1} (methyl orange). The chemical structure of the catalytic system was found to be highly stable during reaction and no metal leaching was detected in reaction medium, evidencing adaptability of cellulose nanocrystals in immobilizing noble metal nanoparticles.

Received 22nd October 2022
Accepted 6th December 2022

DOI: 10.1039/d2ra06689k

rsc.li/rsc-advances

Introduction

During the past decade, many insights into nanoscience and nanotechnology have brought diverse applications of nano-structured objects, in particular in catalytic organic syntheses and catalytic environmental treatments.[1–5] As an important landmark, the catalytic behaviours of nano-objects combine the advantages of traditional homogeneous and heterogeneous catalytic systems, which can be tuned by their size, shape and distribution. In order to prevent the agglomeration leading to an increase in size, metal nanoparticles have been practically dispersed and immobilized in liquid (like ionic liquids,[6–8] polyols,[9–14] water,[14–16] *etc.*) or solid supports.[14,17–19] Taking into account the viewpoint of sustainable development, such catalytic systems have been designed based on biomass-derived supports, such as biochar,[20–22] chitosan[23,24] or cellulose.[25–28] In comparison with well-known inorganic supports relying on their large specific surface area and purposeful porosity, natural-origin materials have been recently introduced in the same framework, thanks to their selective reactivity of available functional groups.

As the most abundant natural biopolymer on earth, nano-celluloses have long-term emerged as a capable platform for diverse purposes.[29–31] In the context of metal nanoparticles applied to catalysis, the alternatives to traditional catalyst supports by using biomass-derived renewable materials, likely nanocelluloses,[25–28] have been paid a great effort, in spite of being less exploited. In plant cell walls, along with hemi-cellulose and lignin, the chains of cellulose are assembled to form microfibrils, which are then bundled together resulting in microfibers and fibers *via* intermolecular hydrogen bonds.[32] Besides highly stable crystalline regions, cellulose possesses

[a]*Faculty of Chemical Engineering, Ho Chi Minh City University of Technology (HCMUT), 268 Ly Thuong Kiet Street, District 10, Ho Chi Minh City, Vietnam. E-mail: dbtrung@hcmut.edu.vn*

[b]*Vietnam National University Ho Chi Minh City, Linh Trung Ward, Thu Duc City, Ho Chi Minh City, Vietnam*

† Electronic supplementary information (ESI) available: Fig. S1 and S2. See https://doi.org/10.1039/d2ra06689k

disordered amorphous regions which are easily penetrated by most of the chemical reagents; as a consequence, nanocrystalline cellulose can be released *via* the breakage of the most accessible glycosidic bonds. In practice, plant-derived nanocelluloses have been mainly fabricated by sulfuric acid hydrolysis or mechanical approach, usually referring to cellulose nanocrystals (CNCs, 30–50 nm in width and 50–500 nm in length, crystallinity index of 54–88%) or cellulose nanofibrils (CNFs, a few hundreds of nano-meters in width and micrometers in length); in which, their size, shape and crystallinity depend on biomass sources and extraction conditions.[29–31]

In addition to well-studied features of nanocelluloses as non-toxicity, biodegradability, good mechanical strength, thermal stability, *etc.*,[29,31] their surface reactivity tuned by a plenty of hydroxyls or specific functionalized groups plays a vital role in the reduction of metal ions towards metal nanoparticles and their immobilization.[25–27] In principle, the electrostatic interactions between surface heteroatoms of such functionalized groups and metal ions precede the electron transfers, leading to fixed anchors of corresponding metal nanoparticles on the surface of nanocelluloses. Therefore, some efforts on modifying the surface of nanocelluloses have been reported, in particular in anionic nanocelluloses modified with aldehyde[33] or carboxyl groups.[34–36] Besides, cationic surfactants were utilized to stabilize metal nanoparticles *via* non-covalent interactions, likely modified with trimethylammonium chloride,[37] hexadecyltrimethylammonium bromide;[38] or *via* coordination with metal ions as using polyethyleneimine.[39] The presence a bilayer containing hydrophobic interactions permits dispersing and immobilizing metal nanoparticles on their surface, thanks to both steric and electronic effects; as a consequence, metal nanoparticles were smaller and better dispersive.

In the framework of nanocelluloses and their application in nanocatalysis, most previous reports focused on either their isolation processes from various plant sources or the utilizing of reported/commercial cellulosic resources for the immobilization of metal nanoparticles.[25–40] To the best of our knowledge, there are very few reports on the isolation of cellulose nanocrystals (previously reported on cellulose nanofibrils (CNFs)) from residual biomass, their full characterization and their direct application in immobilizing metal nanoparticles for catalysis. Therefore, there is still a room for developing and generalizing a comprehensive route as a sequential circuit: (i) isolation and full characterization of cellulose nanocrystals (CNCs) from corn leaf, an agricultural residual biomass; (ii) immobilization of silver nanoparticles on cellulose nanocrystals (AgNPs/CNCs) without using any additional stabilizers or surfactants; (iii) evaluation of catalytic activity and chemical stability of AgNPs/CNCs in the selective reductions of 4-nitrophenol and methyl orange in water at room temperature.

Experimental

Cellulose nanocrystals (CNCs) were isolated from corn leaf *via* a chemical treatment procedure, involving alkalizing, bleaching and acid hydrolysis. Corn leaves were harvested in Tay Ninh province (Vietnam), and then washed, grinded, air dried at 80 °C overnight. The preconditioned material (5.0 g) was firstly treated in 100 mL of NaOH solution at 80 °C under vigorous stirring. After filtration, the solid was washed with copious amounts of deionized water until it was got rid of alkali. Afterwards, the bleaching with 100 mL of H_2O_2 solution (H_2O_2/water = 1/1, v/v) at room temperature was fulfilled overnight. Lastly, the obtained solid was hydrolysed in 100 mL of 1.0 M H_2SO_4 solution at 80 °C under continuous agitation for 6 hours. The final mixture was centrifuged and continuously washed by addition of deionized water to reach pH 7. The neutralized product was also sonicated in deionized water for 30 minutes.

After each stage, the cellulose isolation efficiency was evaluated by Fourier-transform infrared spectroscopy (FT-IR) and the crystallinity index (I_C) of obtained products estimated from powder X-ray diffraction (XRD) (eqn (1)).[41] In which, the alkaline treatment was investigated on various conditions, involving NaOH concentration (0.5–2.0 M), and treatment time (1–6 hours).

$$I_C\ (\%) = \frac{I_{\text{crystalline}} - I_{\text{amorphous}}}{I_{\text{crystalline}}} \times 100 \quad (1)$$

where: $I_{\text{crystalline}}$ and $I_{\text{amorphous}}$ = the maximum diffraction intensity representing the crystalline phase (2θ of 22–24°) and the minimum diffraction intensity representing amorphous phase (2θ of 18–19°).

Silver nanoparticles (AgNPs) were immobilized on preformed cellulose nanocrystals (pre-sonicated in 50 mL deionized water for 30 minutes) *via* the chemical reduction of $AgNO_3$ (0.10 g dissolved in 50 mL deionized water) using $NaBH_4$ (0.1250 g dissolved in 50 mL deionized water) at room temperature for 1 hour. After centrifuging and washing with copious amounts of deionized water and ethanol, the product was air dried overnight to obtain the grey solid (namely AgNPs/CNCs) for further characterizations.

The catalytic activity of AgNPs/CNCs was examined in the selective reductions of 4-nitrophenol (4-NP, 10.0 ppm) towards 4-aminophenol (4-AP) in water and methyl orange (MO, 10.0 ppm) towards aromatic amine derivatives in water, using $NaBH_4$ (mole ratio of 250/1 *vs.* 4-NP or MO) as a reducing agent at room temperature. During 5 minutes, the absorbances of the reaction solutions were monitored by Ultraviolet-visible spectroscopy (UV-vis) in the wavelength range of 200–700 nm, using a 1 cm pathlength quartz cuvette. The calibration curves were constructed with the standard solutions of 4-NP and MO (in the concentration range up to 10.0 ppm) and the corresponding maximum absorbances measured at 400 nm and 465 nm, respectively.

Results and discussion

Efficiency of cellulose isolation from corn leaf

In general, the extraction of cellulose microfibrils from the plant cell wall could be occurred using alkali agents, removing most of the natural impurities, waxes, pectin, the hemicellulose and lignin components, and degrading fatty acids.[30,31,42,43] In fact, lignin was easily denatured under high temperature; in alkaline environment, the ester bonds between lignin and

hemicellulose could be broken, turning the colour of the reaction solution into dark-yellow. Besides, hemicellulose was easily accessible, dissolved and hydrolysed towards monomers, due to its free functional groups, poorly shaped structure, and low polymerization. In caustic soda 18–24%, hemicellulose was soluble,[44] but natural cellulose could not be dissolved.

Next, the purpose of H_2O_2 bleaching was to continuously remove the products from the previous alkalizing (a part of remained lignin and hemicellulose, phenolates and coloured compounds on the surface of cellulose), brightening cellulose fibers and thus being more easily attacked in the further acid treatment. Obviously, H_2O_2 is a strong oxidizing agent, capable of destroying the chemical bonds between hemicellulose and lignin, weakening the physicochemical interactions between these components, degrading the remained lignin components. However, such a bleaching should be gentle, to avoid oxidation and decomposition of unwanted products. Therefore, it was possible to perform a slow oxidation with H_2O_2 agent at room temperature.

As a natural polymer in the form of microfibril bundles consisting of nanometer-sized fibers, cellulose fibers contain structural defects and amorphous regions, which are weak points for acid attacks, hydrolysing cellulose chains into smaller fragments.[30,31,42,43] The acid hydrolysis of cellulose can be repeated until reaching nanoscale sizes. Under H_2SO_4 treatment, cellulose was swell strongly, and the acid agent attacked the crystalline region, partially destroying the hydrogen bonds between the cellulose molecular chains, causing the separation of molecules from each other. In which, the cleavage of the glycosidic bonds between the two anhydroglucose units could be catalysed by the H^+ ions, at high temperatures.[45]

Briefly, the alkaline hydrolysis of corn leaf was firstly carried out at 80 °C; at the temperatures below 100 °C, cellulose was unaffected. The effect of alkali agents and reaction conditions (NaOH concentrations of 0.5–2.0 M and treatment time of 1–6 hours) on cellulose isolation efficiency was evaluated *via* the crystallinity index (I_C) of obtained cellulose estimated from powder X-ray diffraction (XRD) (Table 1), suggesting the optimal conditions of 1.0 M NaOH and 1 hour for the crystallinity index of 61.2%. The bleaching was fulfilled with H_2O_2 solution at room temperature overnight and the acid hydrolysis was performed using 1.0 M H_2SO_4 solution at 80 °C for 6 hours. After each treatment stage, the crystalline structure of cellulose was characterized by XRD, showing the appearance of diffraction peaks corresponding to the crystalline planes (1$\bar{1}$0), (110), (200) and (004) of cellulose I (Fig. 1), in agreement with the standard XRD pattern of cellulose (Fig. S1†).[46] The crystallinity index of untreated raw material (38.4%) and cellulose obtained in each treatment stage showed the efficiency of hemicellulose and lignin removal from corn leaf: the higher the crystallinity index was, the greater the cellulose content was (Table 1). This result was in agreement with more obvious appearance of the diffraction plane (004) after each treatment stage. Besides, the crystallinity index of 61.2% (after alkalizing) was quite equivalent to those after bleaching (61.6%) and acid hydrolysing (67.3%). It can be seen that the crystallinity index of obtained cellulose was mainly determined from the alkalizing (61.2% *vs.* 38.4% of untreated raw material), which efficiently removed amorphous regions from chemical components other than cellulose. In fact, cellulose has both amorphous and crystalline regions; meanwhile, hemicellulose and lignin are amorphous.[47] In short, hemicellulose and lignin were mostly removed after the alkalizing. In the acid hydrolysis, cellulose chains were broken into smaller fragments, removing the amorphous regions of cellulose and leading to a slight increase in crystallinity index (67.3%). The crystallinity index of obtained cellulose was in the range of 54–88% corresponded to cellulose nanocrystals.[29–31]

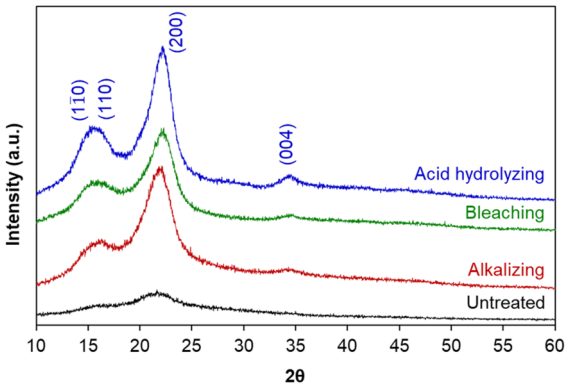

Fig. 1 XRD patterns of untreated raw material and cellulose obtained in each treatment stage.

Table 1 The crystallinity index of untreated raw material and cellulose obtained in each treatment stage estimated from XRD results

Treatment stage	Reaction conditions		I_C (%)
Untreated	—		38.4
Alkalizing	NaOH (M), 80 °C, 1 h	0.5	52.1
		1.0	61.2[a]
		2.0	60.2
	1.0 M NaOH, 80 °C, time (h)	1	61.2[a]
		3	62.0
		6	62.1
Bleaching	H_2O_2 (1/1, v/v), room temperature, overnight		61.6
Acid hydrolyzing	1.0 M H_2SO_4, 80 °C, 6 h		67.3

[a] Selected for further bleaching and acid hydrolysing.

The differences in chemical compositions of untreated raw material and obtained cellulose (after alkalizing and acid hydrolysing) were also examined on vibrational bands of functional groups from Fourier-transform infrared (FT-IR) spectra (Fig. 2). The broaden band at 3400 cm^{-1} was typical for the strong oscillations of the O–H groups, demonstrating the hydrophilicity of the plant fibers.[48] Furthermore, the band at 1640 cm^{-1} was related to the O–H bending vibration from water molecules adsorbed by hydrophilic groups, coming from intermolecular hydrogen bonds between the O–H groups of plant components and water molecules in the air.[49] The band at 2900 cm^{-1} showed the stretching vibration of C–H bonds in

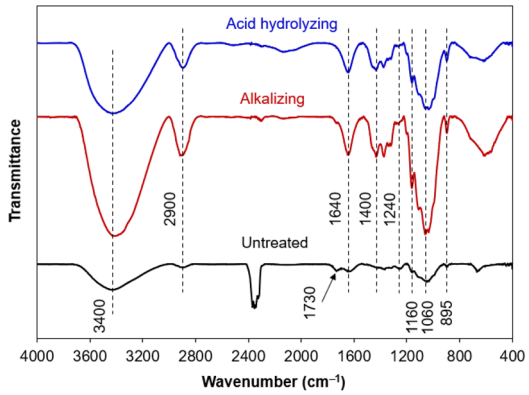

Fig. 2 FT-IR spectra of untreated raw material and cellulose obtained in each treatment stage.

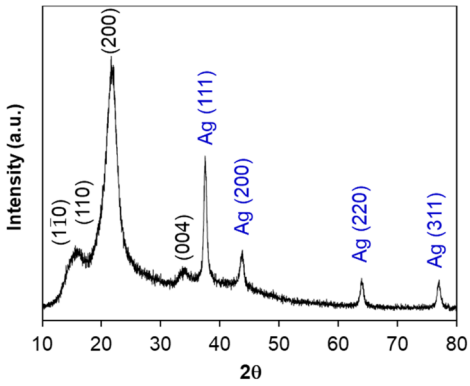

Fig. 3 XRD pattern of AgNPs/CNCs.

most organic components (cellulose, hemicellulose and lignin).[50] In addition, some characteristic bands related to cellulose were observed, involving the band at 1400 cm^{-1} (the C–H and C–O bending vibrations from polysaccharides), the band at 1200–950 cm^{-1} (the stretching vibrations of C–O bonds), the band at 1060 cm^{-1} (the asymmetric bending vibration of the C–O–C ether bond from the pyranose rings in polysaccharides), the band at 895 cm^{-1} attributed to the β-glycoside linkage oscillations (the C–H combined with O–H bending vibrations) between glucose units of cellulose.[51]

In general, the FT-IR spectra has obvious differences between untreated raw material and obtained cellulose. The vibrational bands derived from cellulose could be observed on all the samples, with an increase in intensity through each chemical treatment, in agreement with an increase in cellulose composition. The characteristics of hemicellulose and lignin appeared in untreated raw material, gradually disappeared after alkalizing, and even absolutely disappeared after acid hydrolysis. Typically, the band at 1730 cm^{-1} (acetyl and ester groups from hemicellulose, or carboxyl group of ferulic acid and *p*-coumaric acid from lignin) and the band at 1240 cm^{-1} (the out-of-plane vibration of aryl group from lignin) were observed on untreated raw material and then extinguished after chemical treatments, evidencing the efficient removal of hemicellulose and lignin components from cellulose.[51] Briefly, the isolation of cellulose from corn leaf was successfully occurred by such a chemical treatment, in which the alkaline hydrolysis was of vital importance in removing most organic impurities other than cellulose and determining the crystalline structure of cellulose.

Characteristics of silver nanoparticles immobilized on cellulose nanocrystals

During acid hydrolysis, the cleavage of the glycosidic bonds between the two anhydroglucose units was occurred; in consequence, nanosized cellulose could be obtained from larger cellulose chains.[45] In this part, the size, shape and composition of cellulose nanocrystals were investigated, along with the immobilization of silver nanoparticles on their surface (namely AgNPs/CNCs).

Firstly, the chemical reduction of Ag(I) ions towards Ag(0) was carried out in the presence of cellulose nanocrystals as supports and $NaBH_4$ as a reducing agent at room temperature. The colour of the reaction mixture turned from white to grey, evidencing the formation of silver nanoparticles. The crystalline structure of AgNPs/CNCs was characterized by XRD technique (Fig. 3). Besides the diffraction characteristics of cellulose as the above XRD analysis, the diffraction peaks recorded at 2θ of 37.5°, 43.7°, 63.9° and 77.0° were respectively attributed to the planes (111), (200), (220) and (311) of zero-valent silver bulk with face-centered cubic crystalline structure, in agreement with the standard XRD pattern of silver (Fig. S1†). Using the Scherrer equation, the average crystallite sites of AgNPs and CNCs (AgNPs/CNCs) estimated from the crystalline planes with the maximum intensity were 15.5 nm and 4.2 nm, respectively. Besides, with the sample of CNCs, the average crystallite site was 4.1 nm, in agreement with the results of cellulose I as reported by Li *et al.*[46] According to Bragg's law applied to a cubic system, the lattice constant of silver calculated on the crystalline plane (111) with *d*-spacing (inter-planar spacing) of 2.39776 Å was 4.1530 Å, in comparison with the standard value of 4.0861 Å. The absence of crystalline silver hydroxide or silver peroxide could be concluded on this sample.[52] In addition, the crystallinity index of cellulose from AgNPs/CNCs was also estimated to be 70.1%, being quite similar to that from CNCs (67.3%). These results affirmed that the immobilization of AgNPs unaffected the crystalline features of CNCs.

The elemental analysis on the surface of AgNPs/CNCs was examined by energy dispersive X-ray (EDX) mapping technique (Fig. 4). Besides the main elements (C and O) from cellulose, some trace elements (Al, Si, S) originated from biomass or contaminated from additional chemicals, a paramount element of silver was detected, evidencing the well-dispersion of AgNPs on the surface of cellulose nanocrystals. Importantly, the silver content was found to be 5.1 wt% on the surface analysed by EDX, being a bit higher than that of 4.8 wt% in the whole sample analysed by inductively coupled plasma atomic emission spectroscopy (ICP-AES) (Fig. S2†). This result reaffirmed that most proportion of silver was present on the surface of CNCs, mainly in the form of AgNPs.

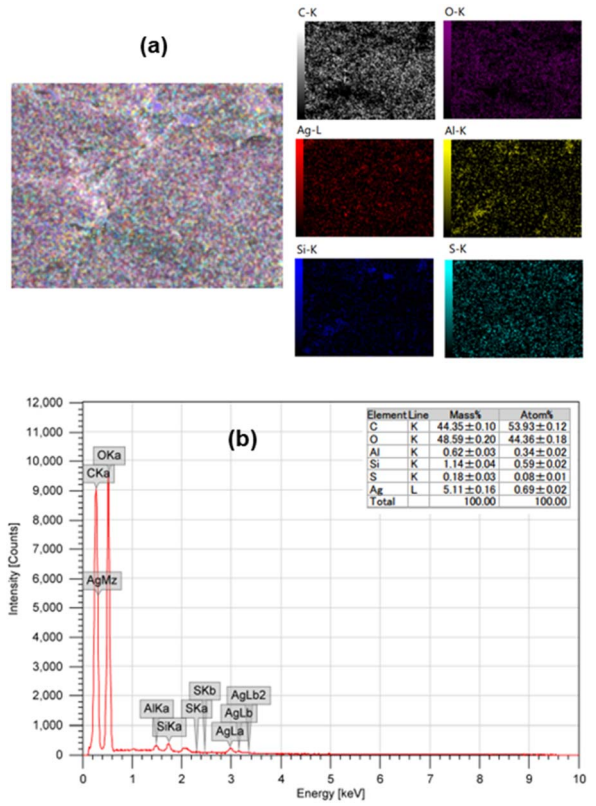

Fig. 4 (a) EDX mapping analysis; (b) EDX spectrum of AgNPs/CNCs.

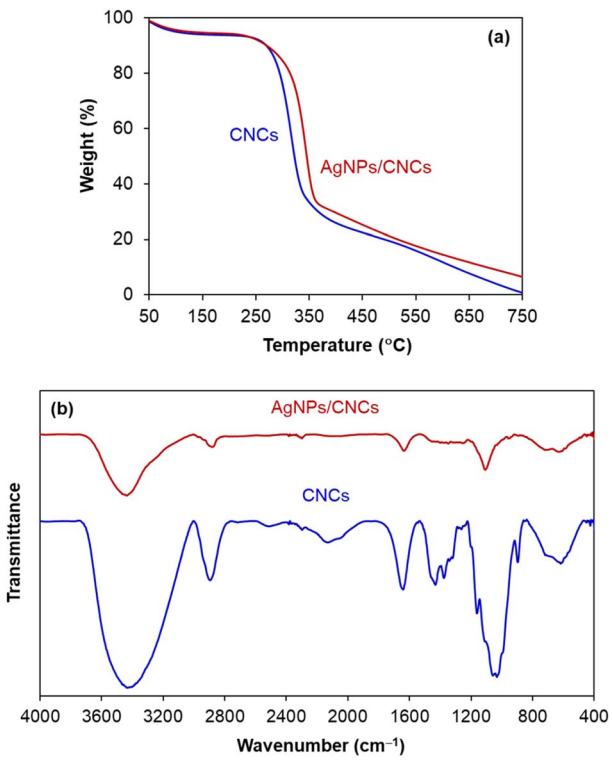

Fig. 5 (a) TGA patterns; (b) FT-IR spectra of CNCs and AgNPs/CNCs.

In order to evaluate thermal stability of CNCs and AgNPs/CNCs, their thermo-gravimetric analyses (TGA) were carried out (Fig. 5a). The mass loss of both samples reached 10 wt% at 250 °C, related to the loss of adsorbed water. Since 250 °C, cellulose was mainly decomposed by heat, and the mass loss of CNCs was always faster than that of AgNPs/CNCs; until the temperature of 750 °C, the difference in mass between such two samples was found to be approximately 5 wt%, being consistent with the silver content previously analysed by EDX and ICP-AES. On the other hand, the unchanged thermal characteristics of AgNPs/CNCs were observed in comparison with CNCs, meaning that the immobilization of AgNPs unaffected the physico-chemical features of CNCs. This result seems to be rational with FT-IR analysis (Fig. 5b); new vibrational bands were undiscovered on AgNPs/CNCs, precluding the presence of silver oxide phase. In contrast to CNCs, the extinction of some vibrational bands on AgNPs/CNCs was probably concerned to atomic-level electrostatic interactions between silver and oxygen of surface functional groups, inhibiting the corresponding vibrational frequencies. In short, AgNPs were well-dispersed on the surface of CNCs without any significant change in their natural surface.

The size and morphology of obtained cellulose after acid hydrolysis were analysed by transmission electron microscopy (TEM) (Fig. 6a), evidencing the formation of cellulose nanocrystals, in the form of nanospheres in shape and 50 nm in diameter. However, cellulose nanospheres showed a tendency in their aggregation into larger chains, due to the supramolecular network possessing intermolecular hydrogen bonds.[53] After immobilizing AgNPs on the surface of CNCs, the system of AgNPs/CNCs showed nanospheres in shape and slightly larger size in comparison with bare CNCs (Fig. 6b). In contrast to

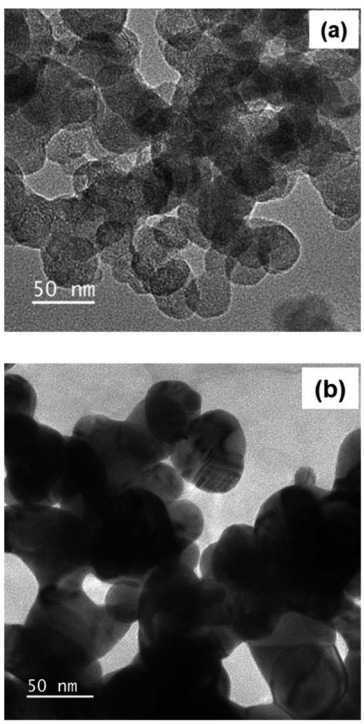

Fig. 6 TEM images of (a) CNCs; (b) AgNPs/CNCs.

previously reported on modifying the surface of nanocelluloses (anionic nanocelluloses modified with aldehyde[33] or carboxyl groups;[34–36] or using cationic surfactants as trimethylammonium chloride[37] or hexadecyltrimethylammonium bromide[38]); in the present work, AgNPs were formed and simply immobilized on the surface of CNCs, thanks to atomic-level electrostatic interactions between silver and oxygen of their nature surface hydroxyl groups[25–27] and their supramolecular network,[53] without using any additional surfactants or stabilizing agents.

Catalytic activity of AgNPs/CNCs in reductions of 4-nitrophenol and methyl orange

The catalytic activity of AgNPs/CNCs was examined in the selective reductions of 4-nitrophenol (4-NP) towards 4-aminophenol (4-AP) and methyl orange (MO) towards aromatic amine derivatives in water, with the assistance of $NaBH_4$ at room temperature. Their conversions were monitored on UV-vis spectra (Fig. 7 and 8) and their corresponding pseudo-first-order kinetic models were also investigated (eqn (2)).

$$\ln\frac{A_t}{A_0} = \ln\frac{C_t}{C_0} = -kt \quad (2)$$

where: A_0 and A_t; C_0 and C_t = the absorbances and concentrations of 4-NP or MO at the initial and a particular time interval; k = the apparent kinetic rate constant; t = time.

In fact, such catalytic reductions have been widely admitted according to Langmuir–Hinshelwood mechanism.[54–59] For instance, in alkaline environment, 4-NP is present in the form of 4-nitrophenolate; the adsorption of such ions on the catalytic active sites occurs prior to the electron transfer towards the nitro groups, reducing into 4-AP as the exclusive product.[54–56] The conversion of 4-NP (the absorbance recorded at the wavelength of 400 nm) towards 4-AP (the absorbance recorded at the wavelength of 300 nm) was monitored in 2 cases: using various silver catalyst concentrations for 5 minutes, and using silver catalyst concentration of 0.125 g L^{-1} for various reaction times (Fig. 7a and b). Normally, the decrease in absorption intensity at 400 nm was rationally correlated to the increase in absorption intensity at 300 nm, meaning that the concentration of 4-AP raised with larger catalyst amount and longer reaction time. After 5 minutes, the conversion of 4-NP reached 90%, with a turnover frequency (TOF) of 670 mmol 4-NP mol Ag^{-1} h^{-1} using 0.125 g L^{-1} silver catalyst and the reaction solution turned

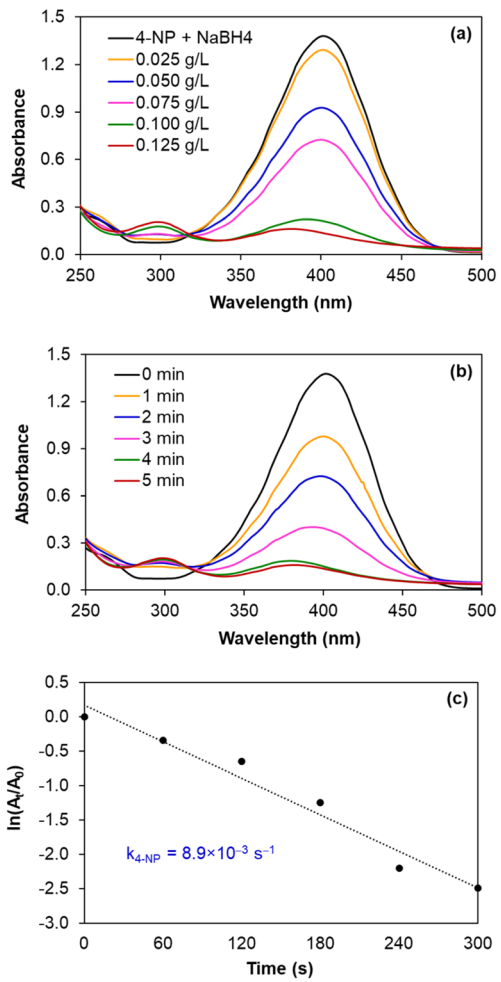

Fig. 7 Monitoring the reduction of 4-NP catalysed by AgNPs/CNCs, with the effects of silver catalyst concentration and reaction time.

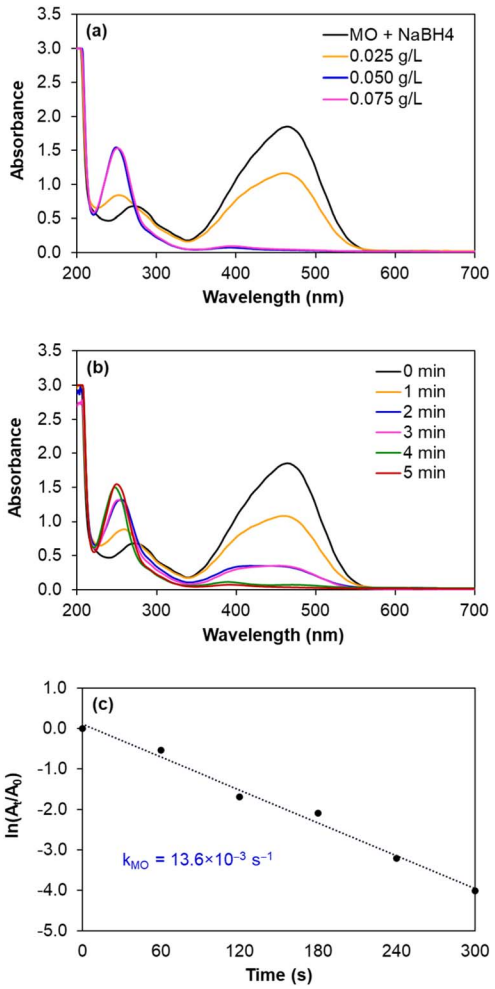

Fig. 8 Monitoring the reduction of MO catalysed by AgNPs/CNCs, with the effects of silver catalyst concentration and reaction time.

from yellow to colourless. As a blank test, the reduction of 4-NP was not afforded in the absence of AgNPs/CNCs or in the presence of only CNCs, proving the silver active sites as nanocatalysts. More importantly, the exclusive product of 4-AP from such a reduction could be derived, evidenced by the presence of the isosbestic points recorded at 275 nm and 320 nm.[54–56] According to a kinetic study, the use of $NaBH_4$ being much greater than 4-NP resulted in the compliance of such a reduction on the pseudo-first-order kinetic model, inspected by plotting $\ln(A_t/A_0)$ against reaction time (Fig. 7c). From such a straight line, the apparent kinetic rate constant of 8.9×10^{-3} s^{-1} was estimated for the reduction of 4-NP. In a similar approach to study the reduction of MO in water, the conversion of MO reached 98%, with a turnover frequency (TOF) of 775 mmol MO mol Ag^{-1} h^{-1} using 0.050 g L^{-1} silver catalyst for 5 minutes, with the colour change of the reaction solution from orange to colourless. The UV-vis spectra of the reaction solutions displayed the absorbance at 465 nm related to the azo group (from MO) and the absorbance at 250 nm attributed to the amino group (from aromatic amine derivatives as reduction products) (Fig. 8a and b).[57–59] The reduction of MO was also reported to obey the pseudo-first-order kinetic model with the rate constant of 13.6×10^{-3} s^{-1} (Fig. 8c). In comparison with 4-NP, the reduction of MO was more efficient under milder conditions and showed the higher reaction rate. In fact, the better electrophilicity of the azo group (−N=N− from MO) than that of the nitro group ($-NO_2$ from 4-NP), facilitating the electron attack to obtain the corresponding reduction products.

In principle, the immobilization of metal nanoparticles on solid supports aims to disperse and prevent their agglomeration, in particular ease in their separation for recycling. Therefore, after each batch experiment, AgNPs/CNCs were separated from the reaction mixture and reused until the 5th run of the reduction of MO, preserving their catalytic activity with insignificant change in MO conversion (Fig. 9a). As expected, the crystalline structure of AgNPs/CNCs was highly stable, with their unchanged compositions as proven by XRD analysis (Fig. 9b). Furthermore, no metal leaching was detected in the reaction medium, analysed by ICP-AES technique. These results reaffirmed the heterogeneity of the catalytic system, in which cellulose nanocrystals were of vital importance in immobilizing AgNPs.

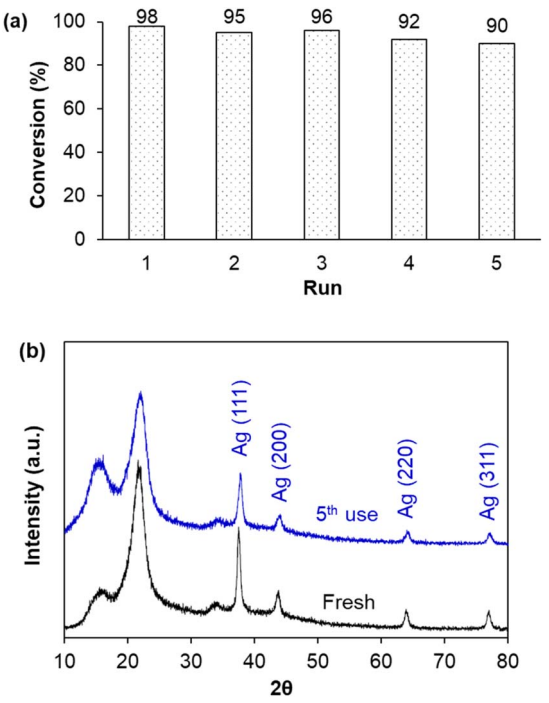

Fig. 9 (a) Reusability of AgNPs/CNCs for the reduction of MO in 5 min; (b) XRD patterns of fresh and 5th used AgNPs/CNCs.

Conclusions

The present work proposed a simple, convenient and well-controlled procedure for the isolation of cellulose nanocrystals from corn leaf, an agricultural residual biomass, in which the alkaline hydrolysis determined their crystalline quality and the acid hydrolysis determined their size and morphology. The immobilization of silver nanoparticles could be obtained on the surface of cellulose nanocrystals thanks to atomic-level electrostatic interaction between silver and oxygen of surface hydroxyls, without using any additional surfactants or stabilizers. The nanocellulose-supported silver nanoparticles evidenced a potential catalytic nano-system in such selective reductions; in particular, their high chemical stability during reaction and no metal leaching reaffirmed the adaptability of cellulose nanocrystals in immobilizing noble metal nanoparticles, thanks to their supramolecular network containing intermolecular hydrogen bonds. These promising results permit us fabricating metal nanoparticles-containing nanocellulose-membrane, which is currently underway.

Conflicts of interest

There are no conflicts to declare.

Acknowledgements

We acknowledge Ho Chi Minh City University of Technology (HCMUT), VNU-HCM for supporting this study.

References

1 K. Philippot and A. Roucoux, *Nanoparticles in Catalysis: Advances in Synthesis and Applications*, Wiley-VCH GmbH, Weinheim, Germany, 2021.
2 P. Serp and K. Philippot, *Nanomaterials in Catalysis*, Wiley-VCH Verlag GmbH & Co. KGaA: Weinheim, Germany, 2013.
3 T. S. Rodrigues, A. G. M. Silva and P. H. C Camargo, *J. Mater. Chem. A*, 2019, **7**, 5857–5874.
4 A. Ohtaka, *Catalysts*, 2021, **11**, 1266.
5 A. Reina, T. Dang-Bao, I. Guerrero-Ríos and M. Gómez, *Nanomaterials*, 2021, **11**, 1891.
6 M. M. Seitkalieva, D. E. Samoylenko, K. A. Lotsman, K. S. Rodygin and V. P. Ananikov, *Coord. Chem. Rev.*, 2021, **445**, 213982.

7 S. Wegner and C. Janiak, *Top. Curr. Chem.*, 2017, **375**, 65.
8 C. Verma, E. E. Ebenso and M. A. Quraishi, *J. Mol. Liq.*, 2019, **276**, 826–849.
9 F. Fiévet, S. Ammar-Merah, R. Brayner, F. Chau, M. Giraud, F. Mammeri, J. Peron, J.-Y. Piquemal, L. Sicard and G. Viau, *Chem. Soc. Rev.*, 2018, **47**, 5187–5233.
10 I. Favier, D. Pla and M. Gómez, *Chem. Rev.*, 2020, **120**, 1146–1183.
11 T. Dang-Bao, I. Favier and M. Gómez, Metal Nanoparticles in Polyols: Bottom-up and Top-down Syntheses and Catalytic Applications, in *Nanoparticles in Catalysis: Advances in Synthesis and Applications*, ed. K. Philippot and A. Roucoux, Wiley-VCH GmbH, Weinheim, Germany, 2021; pp. 99−122.
12 T. Dang-Bao, C. Pradel, I. Favier and M. Gómez, *Adv. Synth. Catal.*, 2017, **359**, 2832–2846.
13 T. Dang-Bao, C. Pradel, I. Favier and M. Gómez, *ACS Appl. Nano Mater.*, 2019, **2**, 1033–1044.
14 T. Dang-Bao, D. Pla, I. Favier and M. Gómez, *Catalysts*, 2017, **7**, 207.
15 T.-H. Le-Lam, H.-H. Lam, H.-P. Phan, T. Nguyen and T. Dang-Bao, *Mater. Today: Proc.*, 2022, **66**, 2720–2725.
16 A. Denicourt-Nowicki, N. Mordvinova and A. Roucoux, Metal Nanoparticles in Water: A Relevant Toolbox for Green Catalysis in *Nanoparticles in Catalysis: Advances in Synthesis and Applications*, ed. K. Philippot and A. Roucoux, Wiley-VCH GmbH, Weinheim, Germany, 2021; pp. 43−71.
17 M. J. Ndolomingo, N. Bingwa and R. Meijboom, *J. Mater. Sci.*, 2020, **55**, 6195–6241.
18 A. Karczmarska, M. Adamek, S. E. Houbbadi, P. Kowalczyk and M. Laskowska, *Crystals*, 2022, **12**, 584.
19 Y. Lou, J. Xu, Y. Zhang, C. Pan, Y. Dong and Y. Zhu, *Mater. Today: Proc.*, 2020, **12**, 100093.
20 J. Liu, J. Jiang, Y. Meng, A. Aihemaiti, Y. Xu, H. Xiang, Y. Gao and X. Chen, *J. Hazard. Mater.*, 2020, **388**, 122026.
21 S.-F. Jiang, L.-L. Ling, Z. Xu, W.-J. Liu and H. Jiang, *Ind. Eng. Chem. Res.*, 2018, **57**, 13055–13064.
22 R. P. Lopes and D. Astruc, *Coord. Chem. Rev.*, 2021, **426**, 213585.
23 X. Chen, X.-J. Xu, X.-C. Zheng, X.-X. Guan and P. Liu, *Mater. Res. Bull.*, 2018, **103**, 89–95.
24 N. Y. Baran, T. Baran and A. Menteş, *Carbohydr. Polym.*, 2018, **181**, 596–604.
25 G. Biliuta and S. Coseri, *Coord. Chem. Rev.*, 2019, **383**, 155–173.
26 M. Kaushik and A. Moores, *Green Chem.*, 2016, **18**, 622–637.
27 T. Jin and A. Moores, Nanocellulose in Catalysis: A Renewable Support Toward Enhanced Nanocatalysis, in *Nanoparticles in Catalysis: Advances in Synthesis and Applications*, ed. K. Philippot and A. Roucoux, Wiley-VCH GmbH, Weinheim, Germany, 2021; pp. 139−157.
28 Q. Zhang, L. Zhang, W. Wu and H. Xiao, *Carbohydr. Polym.*, 2020, **229**, 115454.
29 B. Thomas, M. C. Raj, K. B. Athira, M. H. Rubiyah, J. Joy, A. Moores, G. L. Drisko and C. Sanchez, *Chem. Rev.*, 2018, **118**, 11575–11625.
30 M. B. Noremylia, M. Z. Hassan and Z. Ismail, *Int. J. Biol. Macromol.*, 2022, **206**, 954–976.
31 D. Trache, A. F. Tarchoun, M. Derradji, T. S. Hamidon, N. Masruchin, N. Brosse and M. H. Hussin, *Front. Chem.*, 2020, **8**, 392.
32 D. Klemm, B. Heublein, H.-P. Fink and A. Bohn, *Angew. Chem., Int. Ed.*, 2005, **44**, 3358–3393.
33 K. Zhang, M. Shen, H. Liu, S. Shang, D. Wang and H. Liimatainen, *Carbohydr. Polym.*, 2018, **186**, 132–139.
34 E. Lam, S. Hrapovic, E. Majid, J. H. Chong and J. H. T. Luong, *Nanoscale*, 2012, **4**, 997–1002.
35 M. Gopiraman, D. Deng, S. Saravanamoorthy, I. M. Chung and I. S. Kim, *RSC Adv.*, 2018, **8**, 3014–3023.
36 Y. Chen, S. Chen, B. Wang, J. Yao and H. Wang, *Carbohydr. Polym.*, 2017, **160**, 34–42.
37 Z. Jebali, A. Granados, A. Nabili, S. Boufi, A. M. B. Rego, H. Majdoub and A. Vallribera, *Cellulose*, 2018, **25**, 6963–6975.
38 X. An, Y. Long and Y. Ni, *Carbohydr. Polym.*, 2017, **156**, 253–258.
39 H.-W. Chien, M.-Y. Tsai, C.-J. Kuo and C.-L. Lin, *Nanomaterials*, 2021, **11**, 595.
40 R. Thach-Nguyen and T. Dang-Bao, *IOP Conf. Ser.: Mater. Sci. Eng.*, 2022, **1258**, 012014.
41 X. Zhang, N. Xiao, H. Wang, C. Liu and X. Pan, *Polymers*, 2018, **10**, 614.
42 I. Siró and D. Plackett, *Cellulose*, 2010, **17**, 459–494.
43 M. Jonoobi, R. Oladi, Y. Davoudpour, K. Oksman, A. Dufresne, Y. Hamzeh and R. Davoodi, *Cellulose*, 2015, **22**, 935–969.
44 C. H. Kim, J. Lee, T. Treasure, J. Skotty, T. Floyd, S. S. Kelley and S. Park, *Cellulose*, 2019, **26**, 1323–1333.
45 Y.-B. Huang and Y. Fu, *Green Chem.*, 2013, **15**, 1095–1111.
46 J. Gong, J. Li, J. Xu, Z. Xiang and L. Mo, *RSC Adv.*, 2017, **7**, 33486–33493.
47 S. Andersson, R. Serimaa, T. Paakkari, P. Saranpää and E. Pesonen, *J. Wood Sci.*, 2003, **49**, 531–537.
48 Z. Wang, Z. Yao, J. Zhou, M. He, Q. Jiang, S. Li, Y. Ma, M. Liu and S. Luo, *Int. J. Biol. Macromol.*, 2019, **129**, 108–1089.
49 M. L. Troedec, D. Sedan, C. Peyratout, J. P. Bonnet, A. Smith, R. Guinebretiere, V. Gloaguen and P. Krausz, *Composites, Part A*, 2008, **39**, 514–522.
50 A. A. Oun and J.-W. Rhim, *Carbohydr. Polym.*, 2015, **127**, 101–109.
51 M. Raza, B. Abu-Jdayil, F. Banat and A. H. Al-Marzouqi, *ACS Omega*, 2022, **7**, 25366–25379.
52 P. A. Ganesh, A. N. Prakrthi, S. S. Chandrasekaran and D. Jeyakumar, *RSC Adv.*, 2021, **11**, 24872–24882.
53 R. J. Moon, A. Martini, J. Nairn, J. Simonsen and J. Youngblood, *Chem. Soc. Rev.*, 2011, **40**, 3941–3994.
54 A. I. Ayad, D. Luart, A. O. Dris and E. Guénin, *Nanomaterials*, 2020, **10**, 1169.
55 W. Raza, Catalytic reduction of 4-nitrophenol to 4-aminphenol in water using metal nanoparticles, in *Sustainable Materials and Green Processing for Energy Conversion* ed. K. Y. Cheong and A. Apblett, Elsevier, 2022; pp. 237−261.
56 Y. R. Mejía and N. K. R. Bogireddy, *RSC Adv.*, 2022, **12**, 18661–18675.

57 A. K. Ilunga, T. Khoza, E. Tjabadi and R. Meijboom, *ChemistrySelect*, 2017, **2**, 9803–9809.
58 R. Vijayan, S. Joseph and B. Mathew, *Part. Sci. Technol.*, 2019, **37**, 809–819.
59 A. Rostami-Vartooni, B. Mirtamizdoust and M. Ghaffari, *Biomass Convers. Biorefin.*, 2022, DOI: **10.1007/s13399-022-02941-z**.